Aerodynamic Methods for High Incidence Missile Design

John E. Fidler* and Michael C. Bateman†
Martin Marietta Aerospace, Orlando, Fla.

This paper describes the generation of empirical aerodynamic methods for high incidence missile design. A unique feature of the approach is the provision of a comprehensive data base for correlation into methods. This base is acquired through wind tunnel l testing of large, specially built, extensively instrumented research models. Tests are carried out over wide, systematically varied ranges of relevant aerodynamic and geometric parameters. The work has produced methods for calculating the aerodynamic characteristics of: low aspect ratio fins, in the Mach number range 0.8-2.2; slender missile bodies at angles of attack to 90° at transonic speeds and including the effects of crossflow Mach and Reynolds numbers; and body plus tail configurations, including tail deflection effects, at angles to 60-90° at transonic speeds.

Nomenclature

A_n = coefficients in power series
A_{BT} = axial force coefficient carried over to body due to presence of tail
AR = aspect ratio
C_1, C_2 = coefficients in power series
C_A = axial force coefficient
Cdc = body crossflow drag coefficient
C_M = pitching moment coefficient
C_N = normal force coefficient
d = body diameter
$f(\pi/2)$ = fin nonlinear normal force coefficient for data correlation
I_{BT} = normal force coefficient carried over to body due to presence of tail
M = Mach number
$R_{T(B)}$ = ratio of normal forces on tail on body and alone
Re = Reynolds number
S = area
xcp = distance to center of pressure location from reference point (usually most upstream point on component), measured along component axis
α = angle of attack
δ = tail deflection (negative, leading edge down)
η = factor accounting for body end effects
λ = fin taper ratio

Subscripts

B = body
BT = body plus tail
c = crossflow
I = related to I_{BT}
nl = nonlinear component
0 = value at zero angle
p = planform
ref = reference value
T = tail alone
$T(B)$ = tail in presence of body
α = denotes differentiation with respect to α

Superscripts

$*$ = critical value

Received May 28, 1974; revision received October 15, 1974. Work performed in part under contracts DAAH03-72-C-0487 with U. S. Army Missile Command, and N00019-73-C-0108 with U. S. Naval Air Systems Command.

Index categories: LV/M Aerodynamics; LV/M Configurational Design; Aircraft Aerodynamics (Including Component Aerodynamics).

*Staff Engineer.
†Senior Engineer.

Introduction

A RECURRING problem in missile engineering is the lack of accurate methods for predicting configuration aerodynamic characteristics at high angles of attack across the speed range. Examination of existing methods[1] shows that the problem is particularly acute in the transonic and low supersonic flow ranges. The situation is aggravated by the long term trend toward increased missile maneuverability and angle-of-attack requirements. This trend is summarized in Fig. 1. It will be seen that, historically, maximum angle requirements have steadily increased. The greatest increase has occurred relatively recently to meet advanced airlaunched system maneuverability requirements. These now dictate angles of attack to 90 and even 180°. Recent work[2,3] has provided a significant contribution to aerodynamic methodology suitable for use at these high angles.

Martin Marietta Aerospace, Orlando Division is engaged in long term work to improve high-angle aerodynamic methodology in general.[4] Methods are constructed for calculating missile aerodynamic characteristics to the highest angles of attack required for design efforts. The difficulties associated with obtaining general solutions to the basic flow equations when flow perturbations are not small, preclude an analytical approach to the work. Instead, an experimental/empirical approach is used, with methods being constructed from data covering the required geometries, angles of attack, and Mach and Reynolds number ranges. A unique feature of the work is the provision of a large body of systematic experimental data to form the basis for method construction. At the inception of the program it was decided

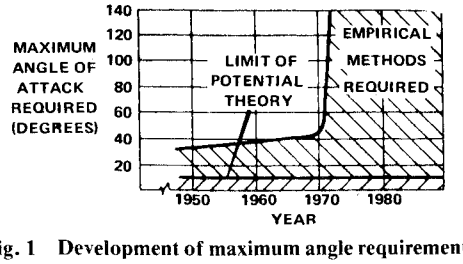

Fig. 1 Development of maximum angle requirements.

to abandon the more usual approach of methodology generation based on data from specific configurations. Such data are too specialized and unsystematic to provide a sound base for general empirical studies. Instead, a large number of extensively instrumented model components were built at the outset and are being tested to provide data over wide, systematically varied values of the relevant geometric and aerodynamic parameters. Empirical methods based on these data should provide adequate high angle methodology for a considerable time to come. This paper outlines the work being carried out at the Orlando Division to upgrade missile aerodynamic technology. Test models, instrumentation, and data generation and reduction are described. The general approach to high angle method construction is discussed and examples presented.

Test Models and Instrumentation

The test models include a large number of wings and tails which may be used with a basic body that can incorporate several different noses and boattails. The tails can also be tested on a reflection plane. Model instrumentation provides information from which the aerodynamic characteristics of complete configurations, configuration components and intercomponent interactions may be determined.

Figure 2 shows the basic body along with a selection of the various components it can accommodate. During testing the body is sting-mounted and accommodates a six-component main balance. The body is 3.75 in. in diameter and has a maximum total length of 54.4 in. Fineness ratio may be varied from 9.5:1 to 14.5 with various boattails and noses deployed. Dimensions of the available noses and boattails are summarized in Table 1. Nose bluntness may be systematically varied.

Of particular interest is the untapered body rear portion. This section accommodates four small strain gage balances arranged in cruciform. A tail is fixed to each balance which then provides tail normal force, hinge moment, and root bending moment. Each balance can be individually rotated to provide data for tails at deflections of $0, \pm 10, \pm 20$, and $\pm 30°$. With the tails undeflected, the balance holder is positioned so that tail trailing edge is at the same axial station as the body base. This is achieved by inserting various spacing pieces forward and aft of the holder. The balances, holders and a selection of spacers are shown along with one set of tails in Fig. 2.

Fifteen different sets of four half-tails, along with the appropriate spacer pieces, are available. All tails have modified double wedge section. Aspect ratio, taper ratio, and body diameter/tailspan for each set are shown in Table 2. The geometry parameters cover the ranges in which current design interests lie. As design interests change, models can be updated by manufacturing additional tails.

The tails may also be tested on the reflection plane shown in Fig. 3. This plane incorporates a tail balance, as well as a motor and gearing system which allows tail angle to be varied between 0 and 180°. Angle of attack is stepped in 30° increments by the plane mechanism. Finer graduations are supplied using the tunnel angle-of-attack system to rotate the entire assembly. In this way, fin angle accuracy is dependent upon tunnel mechanism capabilities.

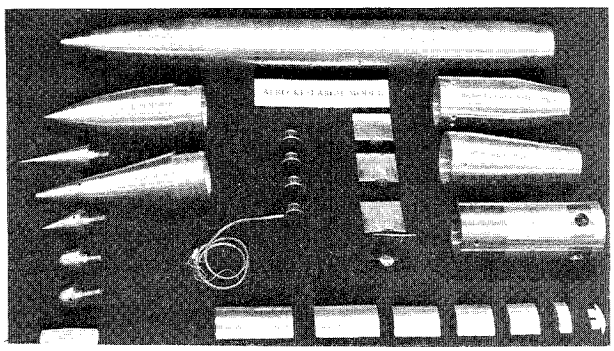

Fig. 2 Basic test body with various components.

Table 1 Summary of model noses and boattails

Nose Section	N1	N2	N3	
Shape	Ogive	Ogive	Ogive	
Fineness ratio	2.5:1	3:1	3:1	
Bluntness ratios	0	0,0.3,0.7	0,0.3,0.7	
Boattail section	B1	B2	B3	B4
Fineness ratio	...	1.0	1.0	2.0
Angle (deg)	0.0	-5.9	-10.0	-5.0
Diameter ratio	1.0	0.8248	0.6472	0.6504

Table 2 Tail model summary

Tails	Aspect ratio	Taper ratio	Body diam / tailspan
1.1	1.0	1.0	0.5
1.2	2.0	0.0	0.4
1.3	2.0	0.5	0.4
1.4	1.0	0.0	0.5
1.5	1.0	0.5	0.5
1.6	2.0	1.0	0.4
2.1	2.0	1.0	0.5
2.2	2.0	0.0	0.5
2.3	2.0	0.5	0.5
3.1	0.5	0.5	0.5
3.2	0.5	1.0	0.5
3.3	2.0	1.0	0.3
3.4	2.0	0.5	0.3
3.5	2.0	0.0	0.3
3.6	0.5	0.0	0.5

Table 3 Wing model summary

Wing	Aspect ratio	Taper ratio	Body diam / wingspan
1.2	2.0	0.0	0.4
1.5	1.0	0.5	0.5
2.1	2.0	1.0	0.5
2.2	2.0	1.0	0.5
2.3	2.0	1.5	0.5
3.1	0.5	0.5	0.5
3.6	0.5	0.0	0.5

The body can also accommodate sets of half-wings mounted in cruciform at several different axial stations between the shoulder and the slotted rear portion. Unlike the tails, the wings are not fixed to recording balances and cannot be deflected. Wings and tails may be deployed simultaneously. Wing geometry is chosen to coincide with current design interests. The complete geometry range is shown in Table 3. All wings have a modified double wedge section.

Data Generation and Reduction

During the course of this program, hundreds of wind tunnel hours were used to generate data on components and configurations. No attempt will be made to present a complete summary of all the bodies, fins, tail angles, roll angles, body-tail, body-wing, and wing-body-tail combinations tested. The generated data have been supplemented by additional information obtained from the European Aerodynamics

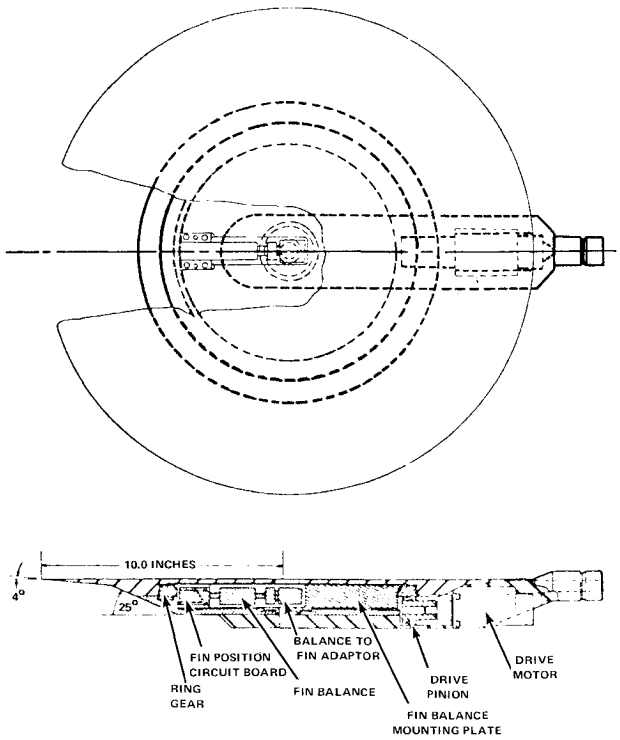

Fig. 3 Reflection plane assembly details.

Working Group[5,6] (Arbeitsgemeinschaft Flugkörper-Aerodynamik).

Data generation usually takes place over the required ranges of angles of attack and Mach number in the following sequence. First, the model body alone is tested and six-component data obtained. Then tails alone are tested on the reflection plane, and three-component data are recorded.

Next, the tails are mounted to the body, and both six- and three-component data are obtained. Finally, tails and wings are deployed on the body and six- and three-component data recorded. With body and tail alone characteristics known, the data are compared with those from the combined body and tail tests to determine the mutual interference quantities between the body and the tails. These include: carry-over loading on body due to presence of the tail, additional tail loading due to carry-over from the body, and tail and body loading from body lee-side vortex effects. With the addition of wings, the previous quantities plus the new data may be used to determine wing trailing vortex interference effects on the downstream portions of the body.

With component basic characteristics and mutual interferences determined, comparisons are then made between the experimental results and those predicted from existing methodology. This reveals areas of method inadequacy. Where methods are inadequate, they are either modified, or replaced with new methods based upon the experimental results. The basic approach here, that of improving deficient methodology empirically, is a traditional solution to the long-standing problem. Usually, however, the available data come from tests on specific configurations. Hence, although the modifications may be adequate for use on comparable geometries, departures from these usually involve remodification of the methods on the basis of the latest configuration data. The unique feature of the present work is the provision of data which systematically cover as many as possible of the foreseeable geometric and aerodynamic parameters of interest to the designer. Thus, the methods have continuous validity, within the ranges of test parameters. If design interest shifts outside the available ranges, further systematic data may have to be generated for method upgrading. The approach will remain the same however with emphasis upon methods having wide applicability.

Aerodynamic Formulations

The instrumentation necessitates the following formulations of pitch-plane aerodynamic characteristics for body/tail "plus" configurations with horizontal tails deflected:

$$C_{N_{BT}} = C_{N_B} + C_{N_T} R_{T(B)} \cos\delta + I_{BT} \tag{1}$$

$$\frac{C_{N_{T(B)}}}{C_{N_T}} = R_{T(B)} \tag{2}$$

$$C_{M_{BT}} = xcp_B C_{N_B} + xcp_{T(B)} C_{N_T} R_{T(B)} \cos\delta + I_{BT} xcp_I \tag{3}$$

$$C_{A_{BT}} = C_{A_B} + C_{N_T} R_{T(B)} \sin\delta + A_{BT} \tag{4}$$

These are somewhat different from the usual forms of the pitch plane equations, mainly because the instrumentation does not specifically measure forces carried over to the body by the tails. To determine $C_{N_{BT}}$, $C_{M_{BT}}$, and $C_{A_{BT}}$, the following quantities are required: C_{N_T}, C_{N_B}, $R_{T(B)}$, $x_{cp_{T(B)}} x_{cp_B}$, I_{BT}, C_{A_B}, $x_{cp_I} A_{BT}$.

Methods have been constructed for calculating these quantities over the angle of attack and Mach number ranges indicated in Table 4. The work was carried out under Government contracts.[7] Several of the devised methods were adopted for use in the U.S. Navy Blunt Body Aerodynamics Handbook.[8]

Methods Construction

The approach to constructing high angle aerodynamic methods is, of necessity, largely empirical. Opportunities seldom arise for use of the well-known correlation parameters of the literature. The small-perturbation flow models from which such parameters are identified are invalid when significant amounts of separated flow are present, i.e., when the angle of attack is greater than a few degrees.

Descriptions are given of the two main types of approach to correlations. The first is based on power series whose boundary conditions are determined analytically, or empirically. Through matching the series with the data, often by means of preserving a free variable, the required correlations are obtained. The second major approach is based on a multidimensional data inspection to determine the relative magnitudes of the various geometry and flow parameters. By producing generalized curves representing the effects of successively weaker parameters, correlations are obtained. Examples of both approaches are described in the next sections.

Isolated Tail Normal Force Coefficient

The power series approach to method construction is exemplified by the technique devised for predicting tail normal force coefficient, C_{N_T}, at angles of attack up to 90°. The

Table 4 Method applicability ranges

Predicted quantity		Angle of attack range (deg)	Mach number range
C_{N_T}		0-90	0.8-2.2
$x_{cp_{T(B)}}$		0-90	0.8-2.2
C_{N_B}		0-60	0.8-1.2
x_{cp_B}		0-90	0.8-1.2
C_{A_B}		0-90	0.8-1.2
$R_{T(B)}$	δ° =	0-60	0.8-1.1
I_{BT}	0	0-60	0.8-1.1
x_{cpI}	-20		
		0-90	0.8-1.1
A_{B_T}	-30	0-60	0.8-1.1

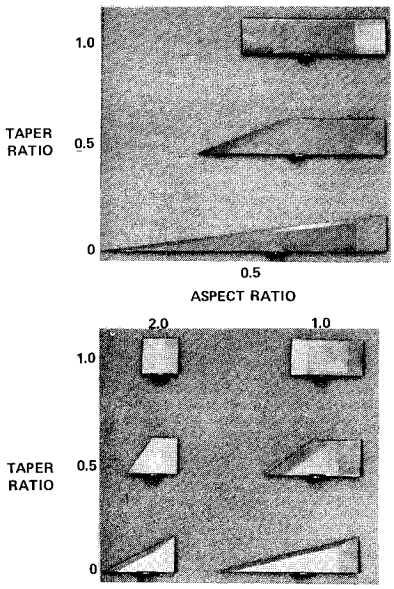

Fig. 4 Fin models tested.

tested tails are shown in Fig. 4. Mach number was varied from 0.8 to 2.2. All tails were deflected to at least 30 or 35° angle of attack with a selected number being deflected to 180°. The higher angle data were sufficient to permit confident extrapolation of the remainder of the data to 90°. Additional inputs were obtained from Ref. 9.

The method developed is similar to the popular crossflow-drag-based methods which are typified by those of Ref. 10. In such methods, the expression for C_{N_T} is assumed given by

$$C_{N_T}=C_1\alpha+C_2\alpha^2 \tag{5}$$

where C_1 is the zero angle normal force curve slope $C_{N_{T_\alpha}}$, and C_2 is a constant, chosen so that the second term forces the overall expression to fit the experimental data. C_2 is termed a "crossflow drag coefficient."

Equation (5) may be regarded as a truncated power series in α. Since it contains two constants, it should fit two boundary conditions on C_N, the condition, C_N $(\alpha=0)=9$ having already been satisfied. One condition is that $(\partial C_N/\partial\alpha)_0$ must equal the normal force curve slope at $\alpha=0$. This determines C_1. The second condition, that of determining the value of C_2, is usually chosen so that the experimental data are fitted at some high angle of attack. The expression is then reasonably accurate up to that angle of attack—provided that the curvature of the data curve always has the same sign. For example, if the curve is initially concave upwards, it must remain so. This is not generally the case for C_N as $\alpha\to 90°$. Furthermore, even at much lower angles of attack, the curvature of the curve can change sign. Hence, in the general case, an expression such as Eq. (5) cannot adequately describe the shape of the normal force curve.

In addition, this form of solution leaves many boundary conditions unsatisfied. For example, at $\alpha=\pi/2$, C_N is a maximum, with $\partial C_N/\partial\alpha=0$; at $\alpha=\pi$, $C_N=0$ and $\partial C_N/\partial\alpha=-(\partial C_N/\partial\alpha)$ at $\alpha=0$ (this last result may be obtained from Slender Body Theory). Hence, since it satisfies none of these latter conditions, Eq. (5) should be expected to further lose accuracy as α is increased towards $\pi/2$ and beyond. An obvious means of improving this situation is to retain the power series form of expansion, but to include as many terms as the boundary conditions permit.

The boundary conditions on C_{N_T} vs α for $\alpha=0$ to 180° are (replacing C_{N_T} with $f(\alpha)$ for convenience and denoting $C_{N_{T_\alpha}}$ by f'). $\alpha=0$, $f(0)=0$, $f'(0)$ predicted by a separate method. $\alpha=180°$, $f(\pi)=0$, $f'(\pi)=-f'(0)$ (potential flow theory result). $\alpha=90°$, $f'(\pi/2)=0$.

At this stage, with five boundary conditions, a power series containing five unknown terms may be used to obtain a more general expression for C_N. The only aerodynamic inputs to this series come from the condition of $f'(0)$ and $f'(\pi)$. Since these quantities are calculable by linearized theory, no guarantee of nonlinearity matching is incorporated. What is required is a further condition which allows the effects of nonlinearities to be empirically accounted for. For this reason, the C_N condition at $\alpha=\pi/2$ has been introduced.

At $\alpha=90°$, $f(\pi/2)$ depends upon the fin planform and Mach number. By leaving the value of $f(\pi/2)$ unspecified in the general expression for the series, it then becomes possible to determine the $f(\pi/2)$ for any combination of AR, λ, and M. This has been done by comparing experimental data with curves calculated using the series.

Power Series Solution

With the six boundary conditions available, a power series containing six unknown coefficients may be used. The power series is assumed to be of the form

$$f(\alpha)=\sum_0^5 A_n\alpha^n$$

from which, with the aid of the boundary conditions, the six unknown constants A_0 through A_5 may be determined. Substitution of boundary conditions and rearrangement of the equation yields:

$$f(\alpha)=f'(0)\alpha+\left\{\frac{16f(\pi/2)}{\pi^2}-\frac{5f'(0)}{\pi}\right\}\alpha^2+\left\{\frac{8f'(0)}{\pi^2}-\frac{32f(\pi/2)}{\pi^3}\right\}\alpha^3+\left\{\frac{16f(\pi/2)}{\pi^4}-\frac{4f'(0)}{\pi^3}\right\}\alpha^4 \tag{6}$$

The term $f'(0)$ is obtained from a separate empirical method. The $f(\pi/2)$ term is obtained through comparison of $f(\alpha)$ with experimental data, Ref. 5.

The values of $f(\pi/2)$ obtained are usually larger than the values of C_{N_c} (Ref. 2). Hence, as the curve approaches 90°, it is necessary to modify the predictions of Eq. (2) so that the curve reaches C_{N_c} there. This is accomplished by means of a second power series which has the general form shown above but uses as boundary conditions the magnitude and slope of the normal force curve at $\alpha=30°$, and $\alpha=90°$. Fairing of the two power series yields the complete normal force curve from 0 to 90°. Such curves can be constructed for any fin using the two power series and the appropriate values of $f(\pi/2)$ and C_{N_c}.

Body Nonlinear Normal Force Coefficient

This force is generated when the boundary-layer separates from either side of a body and rolls up into a vortex pattern on the lee side. The method relates the total force to that acting on unit length of the body C_{d_c} the so-called crossflow drag coefficient. It is usual to determine C_{d_c} from experimental data on two-dimensional cylinders.[12] In the present work, however, the quantity was found from systematic three-dimensional body tests. It is well known[12] that C_{d_c} is a function of the crossflow Mach and Reynolds numbers M_c and R_{e_c}, respectively. Accordingly, the basic body tests were run at the following conditions: a) Constant crossflow Mach number of 0.2, at varying angle of attack and crossflow Reynolds numbers. b) Constant crossflow Reynolds numbers of 0.3×10^5 and 0.6×10^5, constant angle of attack and varying crossflow Mach number. c) Constant freestream conditions and varying angle of attack up to 60°. Freestream Mach number range was 0.8 to 1.3 throughout. Further details may be found in Ref. 4.

Crossflow drag was determined from $C_{N_{nl}}$ the difference between total normal force coefficient and that predicted by potential flow theory, i.e., $C_{d_c}=C_{N_{nl}}\,S_{ref}/\eta\,Sp\,\sin^2\alpha$. The

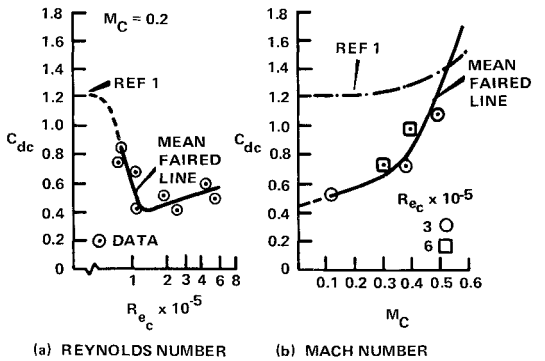

Fig. 5 Effect of crossflow Mach and Reynolds numbers on crossflow drag.

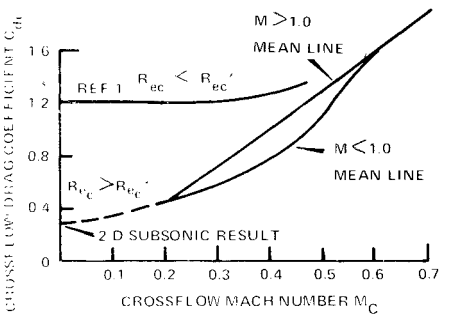

Fig. 6 Variation of crossflow drag with crossflow Mach and Reynolds numbers.

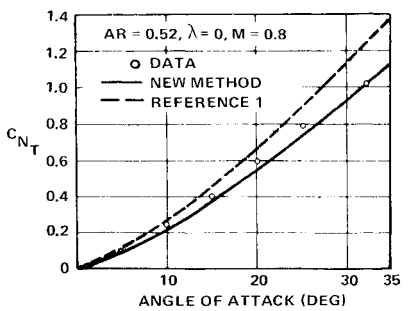

Fig. 7 Comparison of predicted and experimental C_{N_T}.

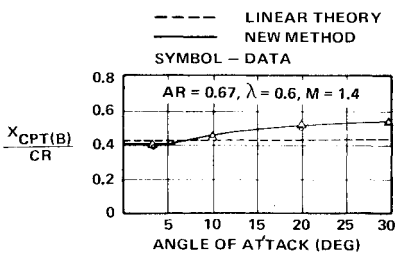

Fig. 8 Comparison of predicted and experimental $x_{cp_{T(B)}}$.

quantity η, which accounts for end effects, was taken from Ref. 1.

Data from tests a) and b) are shown in Figs. 5a and b respectively. The effects of independent variations in Re_c M_c are clearly shown. The so-called critical value of crossflow Reynolds number Re_c* is shown to be about 1×10^5. This is somewhat less than the commonly accepted values of about $2\,5 \times 10^5$ for circular cylinders.[12] 1×10^5 is the critical Reynolds number recommended for use with this method. For subcritical Re_c, the crossflow drag is obtained from Ref. 1. For supercritical Re_c, C_{d_c} is found using the faired data from a), b), and c) previously mentioned. The final, faired curves are shown in Fig. 6. Note that for supercritical separate curves are required for supersonic and subsonic freestream Mach numbers. The results of using this method are illustrated in the next section.

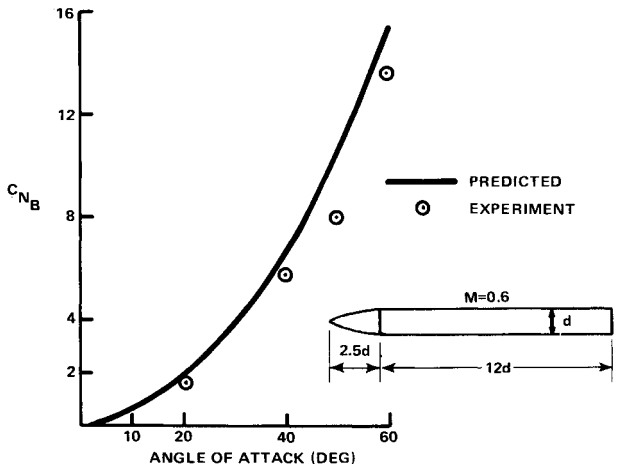

Fig. 9 Comparison of predicted and experimental C_{N_B}.

Method Checkout

Examples will now be given of method predictions compared with independent experimental data. Although the methods extend to high angles of attack, much of the independent data suitable for checkout of all the component and inter-component characteristics were limited to lower angles. This difficulty has been found in other work in the field.[3] A great deal of the detailed data generated for this work are the first of their kind available, especially for bodies with deflected tails. Accordingly, complete checkout of all the methods has yet to be accomplished. However, their performance against independent data is sufficiently satisfactory that checks against higher angle data are expected to pose few problems. A brief discussion accompanies each comparison.

Isolated Tail Normal Force Coefficient, C_{N_T}

Fig. 7 shows that the new method, based on Eq. (6) provides an improvement over the capability of Ref. 1. The data were taken from Ref. 11.

Tail-On-Body Chordwise Center of Pressure Location, $x_{cp_{t(B)}}$

This comparison is shown in Fig. 8. Also shown is the prediction of linearized theory.[13] It will be seen that the new method provides improved capability.

Isolated Body Normal Force Coefficient, C_{N_B}

Figure 9 shows this comparison up to 60° angle of attack. The method includes predictions of both linear and nonlinear components of C_{N_B}, the latter including the effects of crossflow Mach and Reynolds numbers as described earlier.

Isolated Body Center of Pressure Location, x_{cp_B}

Figure 10 shows a comparison of method predictions up to 60° angle of attack (the method is valid to 90°). Matching is quite good overall.

Tail-On-Body Normal Force Coefficient $C_{N_{T(B)}}$

Comparisons are shown in Figs. 11a-d of method predictions and experimental data at angles of attack to 30° while the horizontal tails are deflected 0, -10, -20, and -30°.

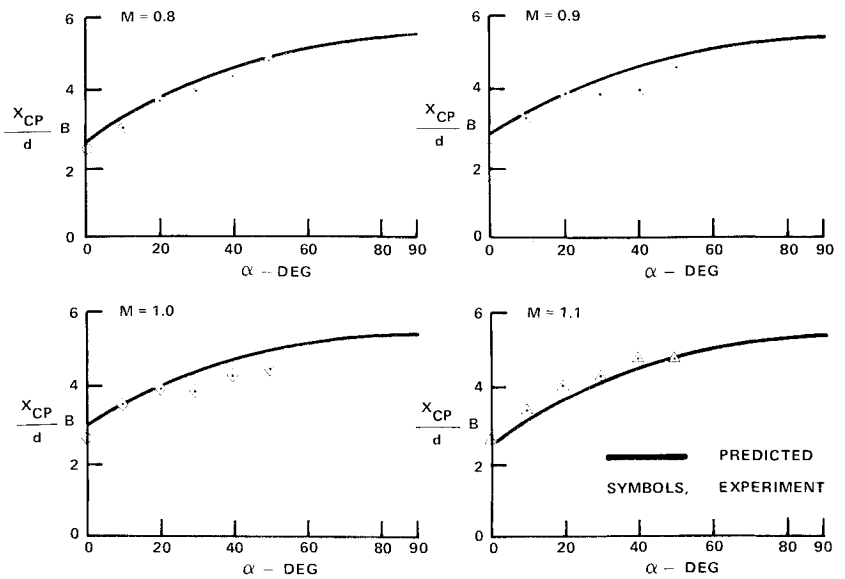

Fig. 10 Comparisons of predicted and experimental $x_{cpB/d}$.

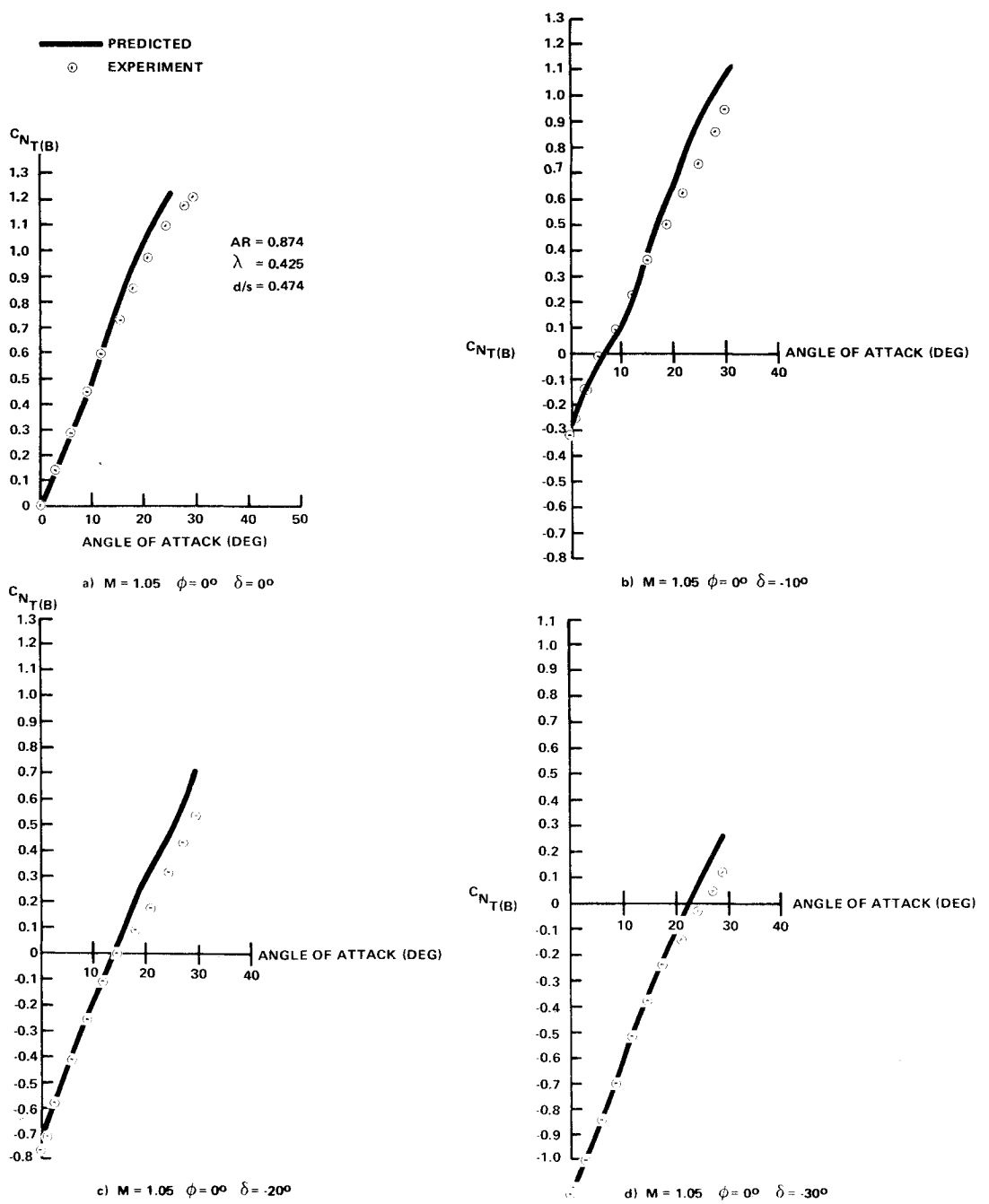

Fig. 11 Comparison of predicted and experimental $C_{N_{T(B)}}$ (various deflections).

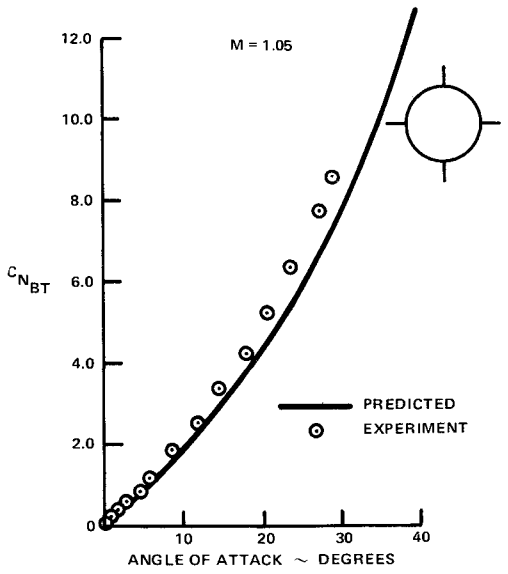

Fig. 12 Comparison of predicted and experimental $C_{N_{BT}}$.

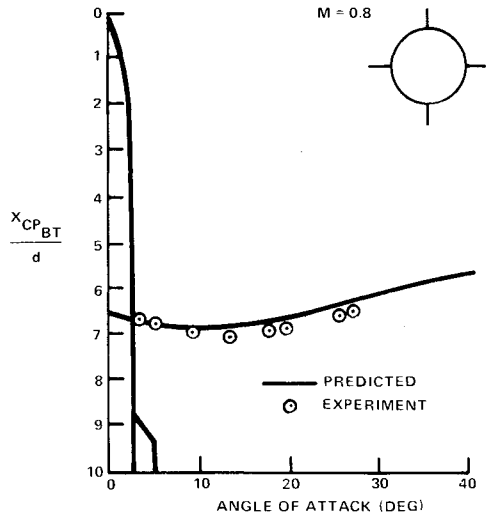

Fig. 13 Comparison of predicted and experimental (xcp_{BT}/d).

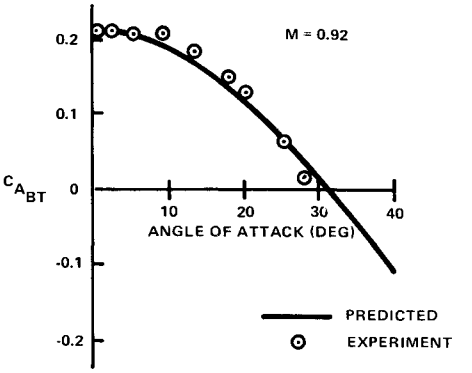

Fig. 14 Comparison of predicted and experimental $C_{A_{BT}}$.

Complete Body/Tail Configuration Normal Force Coefficient

This comparison is shown in Fig. 12 at transonic speed and angle of attack to 30°. Matching is quite good. The methods used were those of Eq. (1).

Complete Body/Tail Configuration Center of Pressure Location xcp_{BT}

This comparison is shown in Fig. 13. Matching is achieved within 0.2 calibers. The methods used were those of Eqs. (1) and (3). The zero angle value was obtained from the slopes of curves of $C_{N_{BT}}$ and $C_{M_{BT}}$.

Complete Body/Tail Configuration Axial Force Coefficient, $C_{A_{BT}}$

This, the final comparison, is shown in Fig. 14. The method takes account of Mach and Reynolds numbers and of the linear and nonlinear components of body axial force.

Conclusions

This paper has described a systematic experimental approach to upgrading missile aerodynamic predictive methods. The angle of attack and speed ranges considered are of direct relevance to modern missile design. It is believed that the methodology improvements described represent a significant advance which could have been obtained in no other way at the present time. Continued use of existing and future systematic models should ensure the timely generation of effective, reliable prediction methods for a considerable time to come.

References

[1] U.S. Air Force Stability and Control Datcom, published by Flight Control Division, Air Force Flight Dynamics Laboratory. Wright-Patterson AFB, Ohio.

[2] Saffell, B. F., Jr., Howard, M. L., and Brooks, E. N., Jr., "A Method for Predicting the Static Aerodynamic Characteristics of Typical Missile Configurations for Angles of Attack to 180 Degrees," R&E Rept. 3645, 1971, Naval Ship Research and Development Center, Carderoek, Md.

[3] Jorgensen, L. E., "A Method for Estimating Static Kerodynamic Characteristics for Slender Bodies of Circular and Noncircular Cross Section Alone and with Lifting Surfaces at Angles of Attack from 0° to 90°, TND-7228, April 1973, NASA.

[4] Fidler, J. E., "A Systematic Experimental Approach to Upgrading Missile Aerodynamic Technology" Ninth U.S. Navy Symposium on Aeroballistics, Applied Physics Lab., Johns Hopkins University, Baltimore, Md., May 1972.

[5] Barth, H. "Datenblätter zur Ermittlung Aerodynamischer Beiwerte Schlanker Bug-Zylinder-Konfigurationen im transsonischen Geschwindikeitsbereich." (Data Sheets for Determining the Aerodynamic Coefficients of Slender Nose Cylinder-Configurations in the Transonic Speed Range), Messerschmitt-Bolkow-Blohm, GMBH, TN WE 12-88/70, Dec. 1970.

[6] Barth, H. "Datenblatter zur Ermittlung von NormalKraft-Momenten - und Tangentialkraftcharackteristiken Schlanker Bug-Zylinder-Konfigurationen im transsonischen Geschwindikeitsbereich." (Data Sheets for Determining the Normal Force, - Moments - & Axial Force Characteristics of Slender Nose-Cylinder-Configurations in the Transonic Speed Range), MBB, TN WE2-97/69, Dec. 1969.

[7] Fidler, J. E. and Bateman, M. C. "Aerodynamic Methodology (Isolated Fins and Bodies)" Final Report on U. S. Army Missile Command Contract DAAH03-72-C-0487, 1972, Redstone Arsenal, Ala.

[8] Darling, J. A., "Handbook of Blunt Body Aerodynamics," NOLTR-73-325, Vol. I, Dec. 1973, Naval Ordnance Lab., Whiteoak, Silver Spring, Md.

[9] Hoerner, S. *Fluid Dynamic Drag*, published by author.

[10] Flax, A. H. and Lawrence, H. F., "The Aerodynamics of Low-Aspect-Ratio Wings and Wing-Body Combinations," Rept. CAL-37, 1951, Cornell Aeronautical Lab., Buffalo, N.Y.

[11] Stahl, W., Hartman, K., and Schneider, W., "Force and Pressure Measurements on a Slender Delta Wing at Transonic Speeds and Varying Reynolds Numbers," Conference on Facilities and Techniques for Aerodynamic Testing at Transonic Speeds and High Reynolds Numbers, AGARD, Preprint 83, 1971.

[12] Jorgensen, L. H., "Prediction of Static Aerodynamic Characteristics for Space-Shuttle-Like and Other Bodies at Angles of Attack from 0° to 180°," TN D-6996, Jan. 1973, NASA.

[13] Pitts, W. C., Nielsen, J. N., and Kaattari, G. E., "Lift and Center of Pressure of Wing-Body-Tail Combinations at Subsonic, Transonic and Supersonic Speeds," Rept. 1307, 1953, NACA.